The Astrophysical Journal Letters, 968:L3 (10pp), 2024 June 10 https://doi.org/10.3847/2041-8213/ad4f7f
© 2024. The Author(s). Published by the American Astronomical Society.
OPEN ACCESS

The Yarkovsky Effect on the Long-term Evolution of Binary Asteroids

Wen-Han Zhou (周文翰)[1], David Vokrouhlický[2], Masanori Kanamaru[3], Harrison Agrusa[1], Petr Pravec[4], Marco Delbo[1], and Patrick Michel[1,5]
[1] Université Côte d'Azur, Observatoire de la Côte d'Azur, CNRS, Laboratoire Lagrange, Nice, France
[2] Astronomical Institute, Charles University, V Holešovičkách 2, CZ 18000, Prague 8, Czech Republic
[3] Department of Earth and Planetary Science, School of Science, the University of Tokyo, Japan
[4] Astronomical Institute, Astronomical Institute of Czech Academy, Ondřejov, CZ-25165, Czech Republic
[5] The University of Tokyo, Department of Systems Innovation, School of Engineering, Tokyo, Japan
Received 2024 April 18; revised 2024 May 16; accepted 2024 May 22; published 2024 June 4

Abstract

We explore the Yarkovsky effect on small binary asteroids. While significant attention has been given to the binary YORP effect, the Yarkovsky effect is often overlooked. We develop an analytical model for the binary Yarkovsky effect, considering both the Yarkovsky–Schach and planetary Yarkovsky components, and verify it against thermophysical numerical simulations. We find that the Yarkovsky force could change the mutual orbit when the asteroid's spin period is unequal to the orbital period. Our analysis predicts new evolutionary paths for binaries. For a prograde asynchronous secondary, the Yarkovsky force will migrate the satellite toward the location of the synchronous orbit on ∼100 kyr timescales, which could be faster than other synchronization processes such as YORP and tides. For retrograde secondaries, the Yarkovsky force always migrates the secondary outward, which could produce asteroid pairs with opposite spin poles. Satellites spinning faster than the Roche limit orbit period (e.g., from ∼4 hr to ∼10 hr) will migrate inward until they disrupt, reshape, or form a contact binary. We also predict a short-lived equilibrium state for asynchronous secondaries where the Yarkovsky force is balanced by tides. We provide calculations of the Yarkovsky-induced drift rate for known asynchronous binaries. If the NASA DART impact broke Dimorphos from synchronous rotation, we predict that Dimorphos's orbit will shrink by $\dot{a} \sim 7\,\mathrm{cm\,yr^{-1}}$, which can be measured by the Hera mission. We also speculate that the Yarkovsky force may have synchronized the Dinkinesh–Selam system after a possible merger of Selam's two lobes.

Unified Astronomy Thesaurus concepts: Asteroids (72); Planetary rings (1254); Solar system (1528)

1. Introduction

Binary asteroids are found throughout the solar system at a wide range of size scales. Their formation mechanisms are also diverse. Kilometer-sized systems are generally thought to form by rotational disruption of the primary resulting from radiative torques (e.g., Walsh et al. 2008), large main-belt systems are thought to form by collisions (e.g., Michel et al. 2001; Durda et al. 2004), while binaries in the Kuiper Belt are thought to be primordial, forming directly from the streaming instability (e.g., Nesvorný et al. 2010). This study primarily focuses on ∼kilometer-sized binaries found among both the near-Earth asteroids (NEAs) and main-belt asteroids (MBAs). These systems are small and close enough to the Sun that radiation forces play an important role in their long-term evolution. Understanding their long-term dynamics is crucial to trace back their evolution and estimate their lifetime, which also provides information on the physical properties and geologic structures of asteroids.

It is widely accepted that the long-term dynamics of binaries are dominated by tides and the binary YORP (BYORP) effect, which is a radiative torque that modifies the orbit of the secondary asteroid (Ćuk & Burns 2005; Vokrouhlický et al. 2015). Tidal dissipation can drive the secondary either outward or inward, depending on whether the secondary's mean motion is slower or faster than the primary's spin (Murray & Dermott 1999). The primaries of binary NEAs typically have short rotation periods, in the range of 2.2–4.5 hr (Walsh & Jacobson 2015), which is likely due to the formation of the system by rotational failure (Pravec & Harris 2007). For simplicity, we assume the primary's spin rate always exceeds the secondary's mean motion and that tides will consequently drive the secondary outward. For small eccentricities, the time evolution of the binary semimajor axis can be written as (Murray & Dermott 1999)

$$\dot{a}_\mathrm{t} = 3\frac{k_\mathrm{p}}{Q_\mathrm{p}}\frac{m_\mathrm{s}}{m_\mathrm{p}}\left(\frac{r_\mathrm{p}}{a}\right)^5 na. \tag{1}$$

Here k_p, Q_p, and m_p are the tidal Love number, quality factor, and mass of the primary, while n, a, and m_s are the mean motion, semimajor axis, and mass of the secondary, respectively. Throughout this manuscript, the subscript "p" denotes the primary, while the subscript "s" denotes the secondary. The nomenclature and symbols are given in Table 2.

While $\dot{a}_\mathrm{t}$ decreases dramatically with the semimajor axis ($\dot{a}_\mathrm{t} \propto a^{-11/2}$), the drift rate caused by the BYORP effect becomes greater with the increasing semimajor axis (Ćuk & Burns 2005; Jacobson & Scheeres 2011; Vokrouhlický et al.

Original content from this work may be used under the terms of the Creative Commons Attribution 4.0 licence. Any further distribution of this work must maintain attribution to the author(s) and the title of the work, journal citation and DOI.

2015). The averaged semimajor axis drift rate under BYORP is

$$\dot{a}_{\rm B} = \frac{2 f_{\rm B} \mathcal{F}}{n}. \quad (2)$$

Here, $f_{\rm B}$ is the dimensionless BYORP coefficient that can be positive or negative, depending on the shape and surface morphology of the secondary.[6] The calculated absolute value of $f_{\rm B}$ for polyhedron asteroid models shows a large range from 10^{-4} to 10^{-1} (Steinberg et al. 2011) with a typical value of 10^{-3} (Jacobson & Scheeres 2011). The nominal radiation pressure per unit mass $\mathcal{F}$ is defined as

$$\mathcal{F} = \frac{\Phi(1-A)\pi r_{\rm s}^2}{m_{\rm s} c}, \quad (3)$$

where $\Phi = 1364\,(a_{\rm h}/{\rm au})^{-2}\ {\rm W\,m^{-2}}$ is the solar flux, A is the Bond albedo, and c is the speed of light. Here $a_{\rm h}$ is the heliocentric orbital semimajor axis of the binary system. The BYORP effect could drive the secondary either outward to an unstable orbit, where external gravitational perturbations would finally destroy the binary system (Ćuk 2007), or inward until the secondary gets tidally disrupted or the BYORP effect is balanced by the tidal effect (Jacobson & Scheeres 2011). The theoretical timescale of the BYORP effect for NEAs is short (e.g., $\leqslant 10^5$ yr; Ćuk & Burns 2005; Ćuk 2007) compared to their dynamical lifetime (e.g., $\sim 10^7$ yr; Gladman et al. 2000), indicating that the observed binary asteroids are either very young or old enough, if they reached a BYORP–tide equilibrium. However, available measurements suggest that binary systems are evolving at much lower rates than predicted by BYORP. The binary asteroid system 1996 FG_3 is observed to have a semimajor axis drift of $-0.07 \pm 0.34\ {\rm cm\,yr^{-1}}$ (Scheirich et al. 2015), which is much lower than the predicted values of $2.3\ {\rm cm\,yr^{-1}}$ (Scheirich et al. 2015) or $7\ {\rm cm\,yr^{-1}}$ (McMahon & Scheeres 2010) based on the secondary shape model. Similarly, based on an available shape model of the secondary, the binary system 1999 KW_4 has been estimated to have a BYORP drift rate of $6.98\ {\rm cm\,yr^{-1}}$ (McMahon & Scheeres 2010) or $8.53\ {\rm cm\,yr^{-1}}$ (Scheirich et al. 2021), while observations of the mutual orbit report an outward drift rate of $1.2\ {\rm cm\,yr^{-1}}$ corresponding to $f_{\rm B} \sim 0.00157$ if tides are neglected (Scheirich et al. 2021). The two orbital solutions for the binary system 2001 SL_9 have drift rates of $\dot{a}$ of $-2.8 \pm 0.2\ {\rm cm\,yr^{-1}}$ or $-5.1 \pm 0.2\ {\rm cm\,yr^{-1}}$ corresponding to $f_{\rm B} = 0.006$ or 0.01, respectively (Scheirich et al. 2021). Since there is no available shape model for the secondary in 2001 SL_9, a theoretical value of $f_{\rm B}$ cannot be derived. The observation data of the Didymos–Dimorphos system before the DART impact show a small drifting rate of $-0.08 \pm 0.02\ {\rm cm\,yr^{-1}}$ (Scheirich & Pravec 2022; Naidu et al. 2024; Scheirich et al. 2024).

Several mechanisms have been proposed for weakening the BYORP effect. The BYORP torque can be weakened, or even removed, by either the nonsynchronous state of the satellite (Ćuk & Burns 2005) or its nonprincipal axis rotation (Quillen et al. 2022). Another possibility is a rotational state referred to as the "barrel instability" (Jacobson et al. 2021), in which the satellite rolls about its longest axis during its orbital motion and its longest axis remains approximately aligned toward the primary (Agrusa et al. 2021). A recent study also suggests that the BYORP coefficient can be reduced by an order of magnitude for satellites like Dimorphos, the secondary of the binary asteroid Didymos, which has an overall "smooth" shape made up of boulders that are all significantly smaller than the size of the body (Ćuk 2023).

In this work, we investigate the Yarkovsky effect that has been largely overlooked in the context of the long-term evolution of binary asteroids. The Yarkovsky effect, which is the radiation force raised on the afternoon side of a rotating object, has been well studied for single asteroids (Vokrouhlický 1998, 1999; Bottke et al. 2006; Vokrouhlický et al. 2015). However, its impact on binary asteroids remains less explored. The Yarkovsky effect on a binary consists of two components: the Yarkovsky–Schach (YS) effect and the planetary Yarkovsky effect. The YS effect is caused by (1) elimination of the satellite irradiation by sunlight when it is located in the primary shadow and (2) the related asymmetric thermal cooling and heating of the secondary after it enters and exits the shadow (in fact, there is also a similar effect on the primary related by the shadow of the secondary, but this produces smaller dynamical perturbation). The YS effect has been studied for Earth satellites (Rubincam 1982, 1987; Milani et al. 1988; Farinella & Vokrouhlický 1996), space debris (Murawiecka & Lemaitre 2018), and Saturn's rings (Rubincam 2006; Vokrouhlický et al. 2007). This effect was noticed for binary asteroids too (Vokrouhlický et al. 2005a) but has not been studied in detail yet. The planetary Yarkovsky effect is simply the Yarkovsky effect caused by the primary's radiation instead of the Sun (Rubincam 2006; Vokrouhlický et al. 2007).

In this Letter, we describe the binary Yarkovsky effect in Section 2 and discuss its implications on the long-term evolution of binary systems in Section 3. The main results are summarized in Section 4.

2. Theory

2.1. Analytical Model

When the secondary enters the shadow of the primary, its surface temperature drops, leading to a reduced Yarkovsky force. After the secondary exits the shadow of the primary, its temperature increases, restoring the Yarkovsky force level before entering the shadow. However, these two processes are not exactly balanced, resulting in a net perturbation over the orbit that leads to a secular change of a. This is the basis of the YS effect, whose concept is displayed in Figure 1. The necessary condition for the YS effect to operate is therefore that the secondary enters the shadow of the primary. This constrains the inclination i between the orbital plane defined by the secondary motion about the primary and the orbital plane of the binary barycenter about the Sun, $i < r_{\rm p}/a$, implying that the satellite crosses the shadow in every orbit about the primary. A nonzero inclination could weaken the YS effect as the time fraction in the shadow decreases with the inclination (Murawiecka & Lemaitre 2018). However, a larger inclination $i > r_{\rm p}/a$ will result in only a fraction of the heliocentric orbit where the secondary can undergo an eclipse and therefore lead to a weakened YS effect. In fact, binary systems that have been discovered tend to exhibit a preferred inclination of approximately 0° or 180° (Pravec et al. 2012). Since the YORP effect

[6] In the literature, the BYORP coefficient is often referred to as B, but we denote it as $f_{\rm B}$ to maintain consistency with other coefficients in this Letter.

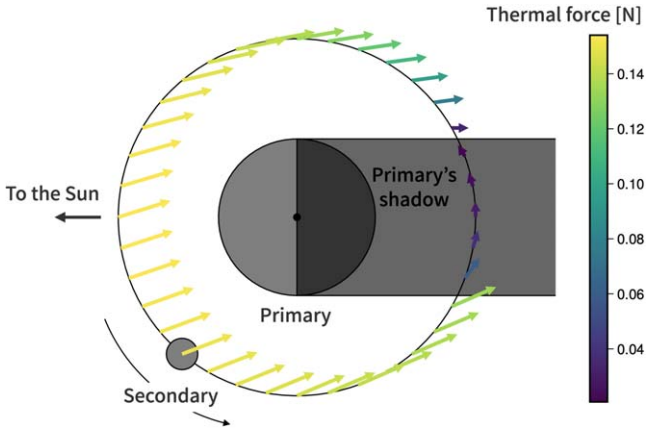

Figure 1. The principle of the YS effect. A binary system consists of a larger primary and a smaller secondary (satellite). The relative orbit is assumed circular, and the satellite has zero obliquity and a rotation synchronous with the motion about the primary; both periods are much smaller than the period of the binary heliocentric motion, such that during one satellite orbit about the primary, the Sun is assumed fixed and in the orbital plane of the satellite. The color-coded arrows attached to the satellite represent its thermal acceleration due to solar irradiation (see also the side bar); the tilt away from the opposite direction to the Sun is due to the satellite thermal inertia. The specific values were computed using the numerical model and binary parameters from Section 2.3. In the absence of the satellite passage through the primary's shadow, the thermal acceleration would be constant. The orbit-averaged effect on the satellite distance from the primary would be zero. The essence of the YS effect is due to the satellite crossing the primary's shadow. The interrupted solar irradiation results in the satellite cooling such that the thermal acceleration drops and tilts. Upon leaving the shadow, the satellite heats, slowly regaining the thermal state at the subsolar configuration. The net budget of the transverse component of the thermal acceleration may be nonzero, depending on the satellite rotation rate and obliquity, resulting in a secular change of its distance from the primary.

drives the primary's obliquity to 0° or 180° (Rubincam 2000), the optimum condition $i < r_p/a$ is usually easily satisfied for small binaries if they form via YORP-driven spin-up and mass shedding followed by reaccumulation in the equatorial plane of the primary (Walsh et al. 2008; Pravec et al. 2012; Agrusa et al. 2024) For simplicity, in the following, we take $i = 0°$. We first develop a simple analytical YS effect model, and later in this section, we justify it by comparison with the results of a numerical simulation.

There is also a "mirror" YS effect related to the satellite shadow that perturbs the thermal state of the primary. In principle, the corresponding drift rate of the satellite semimajor axis $\dot{a}$ may be described by a similar approach used for the core YS effect on the satellite. While algebraic complications would arise due to primary's larger size than the satellite's cross section, it is conceivable that the primary-driven YS component would be a factor of $\sim(r_s/r_p)^2$ smaller than the secondary-driven YS effect. As our ambition is to provide a simple and introductory analytical estimate of the YS effect, we neglect the thermal acceleration of the primary at this moment.

Returning to the analytical formulation of the YS effect for the satellite, we assume that both the primary and the secondary have a spherical shape with radii r_p and r_s, respectively (nonsphericity of both components may result in corrections, which are typically lower than the aimed accuracy of our simple analytical model). The heliocentric orbit of the barycenter and the relative orbit of the two components in the binary are both assumed to be circular. We denote the semimajor axis of the secondary orbit about the primary by a, the corresponding mean motion by n, and the spin rate of the secondary by ω. We introduce the frequency ratio $m = |\omega/(n - n_h)| \simeq |\omega/n|$, where n_h is the heliocentric mean motion of the binary system. In this work, we assume $n_h \ll n$; thus, $n - n_h \simeq n$ in the denominator of m. We assume the secondary is in principal axis rotation. Complex rotational states such as a tumbling state or the so-called barrel instability are left for future investigation.

The complete mathematical solution of the YS effect for a small satellite orbiting a large primary is given in Vokrouhlický et al. (2007; a ring particle about Saturn, in their context). The semimajor axis drift rate of the secondary due to the YS effect has a generic form:

$$\dot{a}_{YS} = \frac{2 f_{YS} \mathcal{F}}{n}. \tag{4}$$

The dimensionless coefficient f_{YS} is called the YS coefficient in this work and depends on the physical properties of the binary system, such as the mutual orbital period, the sizes of the two bodies composing the binary, and the thermal properties. In fact, f_{YS} is the sum of the diurnal component and the seasonal component,

$$f_{YS} = f_{YS,d} + f_{YS,s}, \tag{5}$$

where

$$f_{YS,d} = \frac{4c_1}{9}\left[V(z_{m-1}) \cos^4 \frac{\varepsilon}{2} - V(z_{m+1}) \sin^4 \frac{\varepsilon}{2} \right], \tag{6}$$

$$f_{YS,s} = -\frac{2c_1}{9} V(z_1) \sin^2 \varepsilon. \tag{7}$$

Here $z_{m\pm1} = \sqrt{-\imath(m \pm 1)}\, r_s/l_n$ $(\imath = \sqrt{-1})$, $c_1 \simeq r_p/\pi a$ expresses the orbital fraction spent by the satellite in the primary's shadow, and $V(z)$ is a real-value function defined by

$$V(z) = \mathrm{Im}\left(1 + \chi \frac{z}{j_1(z)} \frac{dj_1(z)}{dz} \right)^{-1}, \tag{8}$$

with $j_1(z)$ denoting the spherical Bessel function of the first kind and order 1,

$$j_1(z) = \frac{\sin z}{z^2} - \frac{\cos z}{z}. \tag{9}$$

The thermal penetration depth l_n at the satellite mean-motion frequency n is given by $l_n = \sqrt{K_s/(\rho_s C_s n)}$, where K_s is the thermal conductivity, C_s is the heat capacity, and ρ_s is the surface density of the satellite. The variable χ is defined as

$$\chi = \frac{K_s}{\sqrt{2}\, r_s \epsilon \sigma T_{sub}^3 c_0^{3/4}}, \tag{10}$$

with $c_0 = 1 - c_1$, the subsolar temperature T_{sub} defined by $\epsilon\sigma T_{sub}^4 = (1 - A)\Phi$, ϵ the thermal emissivity, and σ the Stefan–Boltzmann constant. Alternatively, the $V(z)$ function can be expressed using a real argument $x = \sqrt{2\imath}\, z$,

$$V(z) = \frac{E(x) \sin \delta(x)}{1 + \chi} = \frac{1}{1 + \chi} \frac{B(x)C(x) - A(x)D(x)}{C^2(x) + D^2(x)}. \tag{11}$$

The expressions for functions A, B, C, and D are derived in Vokrouhlický (1998) and are also provided in Appendix B.

Apart from the eclipse-induced YS effect, the radiation from the primary to the secondary would cause a so-called

"planetary" Yarkovsky effect (Rubincam 2006; Vokrouhlický et al. 2007), which replaces the solar radiation with the thermal radiation of the primary in the Yarkovsky effect. Its resulting semimajor axis drift rate can be expressed as

$$\dot{a}_{\rm pY} = \frac{2f_{\rm pY}\mathcal{F}_{\rm pY}}{n}, \tag{12}$$

where

$$f_{\rm pY} \simeq -\frac{f_{\rm YS}}{c_1}, \tag{13}$$

$$\mathcal{F}_{\rm pY} \simeq \mathcal{F}\left(\frac{r_{\rm p}}{2a}\right)^2. \tag{14}$$

Equation (14) results from the fact that the radiation flux from the primary is smaller than the solar radiation flux by a factor of $(r_{\rm p}/2a)^2$. It is important that the planetary Yarkovsky effect does not require the eclipse condition and therefore works for high-inclination cases. Noticing that $c_1 \simeq r_{\rm p}/\pi a$, we have

$$\dot{a}_{\rm pY} = -a_{\rm YS}\frac{\pi r_{\rm p}}{4a}, \tag{15}$$

showing that the planetary Yarkovsky effect is an opposite effect to the YS effect. Considering $r_{\rm p}/a < 1$, the YS coefficient not only dominates over the planetary Yarkovsky effect but also becomes progressively stronger relative to it as the binary semimajor increases.

Combining the eclipse-induced YS effect (Equation (4)) and the planetary Yarkovsky effect (Equation (15)), we obtain the total Yarkovsky effect on the binary asteroid:

$$\dot{a}_{\rm Y} = \dot{a}_{\rm YS} + \dot{a}_{\rm pY} = \dot{a}_{\rm YS}\left(1 - \frac{\pi r_{\rm p}}{4a}\right). \tag{16}$$

For the sake of simplicity, we introduce a combined Yarkovsky coefficient,

$$f_{\rm Y} = f_{\rm YS}\left(1 - \frac{\pi r_{\rm p}}{4a}\right), \tag{17}$$

such that the total Yarkovsky effect has a generic form:

$$\dot{a}_{\rm Y} = \frac{2f_{\rm Y}\mathcal{F}}{n}. \tag{18}$$

2.2. Discussion

The sign of the Yarkovsky-induced drift rate $\dot{a}_{\rm Y}$ is the same as the Yarkovsky coefficient $f_{\rm Y}$, while the latter is a complicated function that depends on the properties of the binary system (see Equations (6) and (7)). Roughly said, for prograde secondaries ($\varepsilon < 90°$), the Yarkovsky effect tends to drive the secondary toward the synchronous orbit $a_{\rm syn}$ determined by $n = \omega$, while for retrograde secondaries ($\varepsilon > 90°$), the Yarkovsky effect always drives the secondary outward until it leaves the system. The Yarkovsky coefficient $f_{\rm Y}$ could have a simpler form in the fast spin regime ($\omega \gg n$) or in the slow spin regime ($\omega \ll n$), as discussed in Appendix C.

For the purpose of an illustration, we consider a binary system on a heliocentric circular orbit and $a_{\rm h} = 1$ au. We set $r_{\rm p} = 1000$ m, $r_{\rm s} = 200$ m, and the physical parameters $K_{\rm p} = K_{\rm s} = 0.1$ W m^{-1} K^{-1}, $C_{\rm p} = C_{\rm s} = 550$ J K^{-1} kg^{-1}, and $\rho_{\rm p} = \rho_{\rm s} = 2000$ kg m^{-3}. The semimajor axis a of the binary components is fixed at 2650 m, which corresponds to an orbital period of 10 hr. As a result, different values of m are obtained solely by changing the spin frequency ω. We also set the obliquity ε as a free parameter. Figure 2 shows the Yarkovsky coefficient $f_{\rm Y}$ as a function of m and ε. Clearly, the Yarkovsky effect drives the secondary orbit to evolve toward the synchronous state ($m = 1$) for prograde rotators but always pushes the retrograde rotators outward. In the blue zone, the Yarkovsky effect maximizes at a spin period of ∼3 hr, corresponding to the thermal parameter value $\Theta_\omega \sim \sqrt{2}$; here $\Theta_\omega = \Gamma\sqrt{\omega}/(\epsilon\sigma T_{\rm sub}^3)$ with the surface thermal inertia $\Gamma = \sqrt{K_{\rm s}C_{\rm s}\rho_{\rm s}}$.

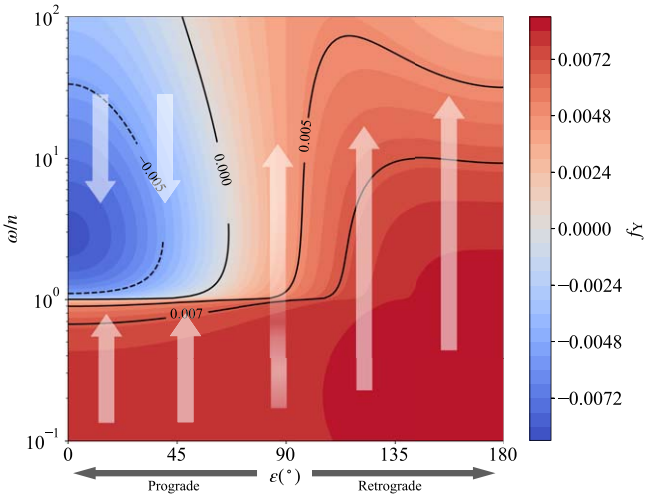

Figure 2. The Yarkovsky coefficient, $f_{\rm Y}$, as a function of m and ε, where $m = \omega/n$ is the ratio of the spin frequency to the orbital frequency and ε is the angle between the spin vector and the orbital vector. The sign of $f_{\rm Y}$ is the same as the sign of $\dot{a}_{\rm Y}$, and $f_{\rm Y} = 0.005$ corresponds to $\dot{a} = 1.4$ cm yr^{-1} for this system. The direction of the white arrows denotes the evolution direction under the Yarkovsky effect. For small values of ε, the Yarkovsky effect drives m toward 1; otherwise, the satellite is driven away from the primary.

In the most common case seen for the observed binary systems, namely, $\varepsilon \sim 0°$, the Yarkovsky coefficient simplifies (with only the diurnal component contributing)

$$f_{\rm YS} = \frac{4c_1}{9}V(z_{m-1}). \tag{19}$$

We introduce the relative angular frequency $\Delta = \omega - n$ such that $z_{m-1} = \sqrt{-\imath}\, r_{\rm s}/l_\Delta$, where l_Δ is defined as

$$l_\Delta = \sqrt{\frac{K_{\rm s}}{\rho_{\rm s}C_{\rm s}|\Delta|}} = 2\ {\rm cm}\left(\frac{|\Delta|}{2\times 10^{-4}\ {\rm rad\ s^{-1}}}\right)^{-1/2} \tag{20}$$

(we use the above-given physical parameters of the satellite surface). In the case of large bodies $r_s \gg l_\Delta$, readily fulfilled in the cases of interest, we can further apply the approximate expression for the $V(z_{m-1})$ function,

$$V(z_{m-1}) = -\frac{\Theta_\Delta}{2 + 2\Theta_\Delta + \Theta_\Delta^2}\,{\rm Sign}(\omega - n), \tag{21}$$

with the thermal parameter Θ_Δ defined as

$$\Theta_\Delta = \frac{\Gamma\sqrt{|\Delta|}}{\varepsilon\sigma T_{\rm sub}^3}. \tag{22}$$

Note that $f_{\rm Y}$ does not depend on the size of the secondary when $r_{\rm s} \gg l_\Delta$. In the regime of $r_{\rm s} < l_\Delta$, $f_{\rm Y}$ gets smaller when $r_{\rm s}$ decreases. The Yarkovsky coefficient $f_{\rm Y}$ depends on the

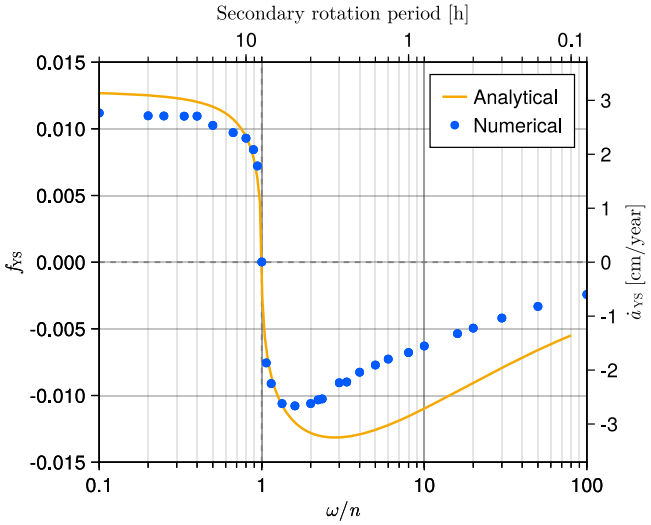

Figure 3. The YS coefficient f_{YS} as a function of the ratio of the spin velocity to the mean motion, ω/n. The blue dots show the numerical results of the zero-obliquity case compared with the analytical solution (orange). The secondary x-axis and y-axis indicate the corresponding rotation period and semimajor axis drift for the given binary system.

semimajor axis following $f_Y \propto r_p(1-\pi r_p/4a)/a$, considering a constant Δ. As the secondary asteroid is always outside the Roche limit ($a \gtrsim 1.5r_p$), f_Y decreases with a.

2.3. Comparison with Numerical Simulation

To validate our analytical solution, we compare our results with numerical solutions. We performed thermophysical simulations using the `AsteroidThermoPhysicalModels.jl` library, one of the functionalities of the asteroid dynamical simulator `Astroshaper` (https://github.com/Astroshaper). This package was originally developed to predict the YORP effect on asteroid 162173 Ryugu, a target asteroid of Japan's Hayabusa2 spacecraft (Kanamaru et al. 2021). The thermophysical model, originally formulated for a single asteroid, has been generalized to include all relevant thermal effects in a binary system. Most importantly, we account for the mutual shadowing between the binary components.

For comparison with the analytical solution, we numerically evaluated the YS coefficients f_{YS} for different orbit and spin periods of the secondary. We consider a binary asteroid with the same parameters as Section 2.2. The binary at 1 au heliocentric distance has been given zero eccentricity (both the heliocentric and mutual orbits). The spherical binary components were approximated using a triangulated model with 2562 vertices and 5120 facets for both the primary and the secondary. The obliquity of the secondary's spin pole is set to be $\varepsilon = 0°$.

We performed thermophysical simulations for 100 thermal cycles to reach converged values of f_{YS}, with the least common multiple of the secondary's orbit period and the spin period as one cycle. The orbital period of the satellite was fixed at 8 hr, and the rotation period was varied to simulate cases of different ω/n. The radiation flux between the primary and the secondary was hereby ignored to save computational time. At each time step, we calculated the temperature distribution of the asteroids and the thermally induced force on each surface facet, as described in Rozitis & Green (2012). The thermal force in an asteroid-fixed frame was then transformed into an inertial frame to calculate the acceleration on the secondary. The effective YS coefficients f_{YS} are plotted in Figure 3 as a function of the ratio of the spin velocity to the mean motion, ω/n. The numerical results are in reasonable agreement with the analytical solution (Equation (21)), given its simplicity, providing its justification. A complete parameter survey by the numerical thermophysical model will be presented in future work.

3. Implications

3.1. Synchronization of the Secondary Component

The majority of the binary asteroid systems are observed to have a synchronized secondary. Simulation of rotational disruption of asteroids shows that the secondary could be born either asynchronous or synchronous due to the frequent reshaping near the Roche limit (Agrusa et al. 2024). Currently, there are two known mechanisms for the synchronization of the secondary asteroid: the tidal effect and the YORP effect. Both of these effects synchronize the secondary by changing the rotation of the secondary until it gets tidally locked. The tidal bulge raised on the secondary by the primary causes a torque that tends to remove the difference between the spin frequency and orbital frequency. The estimate of the characteristic timescale related to the tidal torque makes use of (Murray & Dermott 1999)

$$\dot{\omega} = \frac{5\pi G\rho_p^2 r_p^6}{r_s^5 a \rho_s}\left(\frac{r_s}{a}\right)^5 \frac{k_s}{Q}, \tag{23}$$

with $k_s = 0.038\, G\rho_s^2 r_s^2/\mu$ (Burns & Safronov 1973; Murray & Dermott 1999; Quillen et al. 2022) assuming a monolithic structure. While we note that k_s/Q is a more fundamental parameter for the tidal effect, we use the parameter μQ for ease of comparison with previous work. However, it is important to note that the expression of the tidal Love number k_2 for rubble piles is still under debate and poorly constrained (Burns & Safronov 1973; Yoder 1982; Jacobson & Scheeres 2011; Taylor & Margot 2011; DellaGiustina et al. 2024). The timescale $\tau_{t,spin} \simeq \omega/\dot{\omega}$ reads

$$\begin{aligned}\tau_{t,spin} &= \frac{\omega Q \rho_s}{5\pi k_2 G \rho_p^2}\left(\frac{a}{r_p}\right)^6 \\ &\simeq 10\ \mathrm{Myr}\left(\frac{8.7\ \mathrm{hr}}{P_s}\right)\left(\frac{a/r_p}{2.5}\right)^6\left(\frac{r_s}{0.2\ \mathrm{km}}\right)^{-2}\left(\frac{\mu Q}{10^{11}\ \mathrm{Pa}}\right),\end{aligned} \tag{24}$$

where $P_s = 2\pi/\omega$ is the satellite rotation period. The value of μQ, which varies by a few orders of magnitude in the literature (Burns & Safronov 1973; Goldreich & Sari 2009; Efroimsky 2015; Caudal 2023; Pou & Nimmo 2024), is still uncertain for rubble piles, and its dependence on the size is also poorly known.

The radiative torque due to the irregular shape, namely, the YORP torque, can spin the secondary up or down. The direction of the YORP torque, which depends on the shape and rotation state, is still poorly understood. The timescale of the YORP effect is (Rubincam 2000; Bottke et al. 2006; Marzari et al. 2020)

$$\tau_{YORP} \simeq 42\ \mathrm{kyr}\left(\frac{r_s}{0.2\ \mathrm{km}}\right)^2\left(\frac{8\ \mathrm{hr}}{P}\right)\left(\frac{a_h}{1\ \mathrm{au}}\right)^2. \tag{25}$$

It is obvious that the YORP timescale is much shorter than the tidal timescale, implying that the YORP effect could be the major mechanism for the synchronization of the secondary asteroid. However, there are two issues. First, the YORP effect may be highly sensitive to the fine-scale surface irregularities (Breiter et al. 2009; Statler 2009; Cotto-Figueroa et al. 2015). In most cases, this information is beyond the resolution of the available observations. As a result, predicting even the instantaneous YORP value may be very difficult (this is the reason why the presently achieved YORP detections are often smaller than theoretically expected; see the latest compilation in the discussion section of Ďurech et al. 2024). From a long-term perspective, the movement of boulders (Golubov & Krugly 2012) and formation of impact craters (Zhou et al. 2022; Zhou & Michel 2024) could modify or even reverse the direction of the YORP torque. Building on the YORP's shape sensitivity, Bottke et al. (2015) introduced the "stochastic YORP" concept and showed that it overall weakens the long-term effects of nominal YORP. Second, theoretically, the YORP torque has an equal probability of taking a positive or negative sign. Therefore, we would expect that half of the secondaries are asynchronous due to the wrong direction of the YORP torque (i.e., opposite to $n-\omega$), which is inconsistent with the observed dominating synchronous population with tight orbits (e.g., $a<2.2r_{\rm p}$ or $P_{\rm orb}<20$ hr; see Pravec et al. 2016). Asynchronous secondaries occur more frequently in wide orbits compared to tighter ones (Pravec et al. 2016), implying a correlation to some mechanism that influences orbital configurations.

While there is no clear answer for the dominating mechanism of synchronization of the secondary, we find that the Yarkovsky effect also drives the prograde rotators toward the synchronous orbit (Section 2). Here, we estimate the timescale for the Yarkovsky effect to synchronize the orbit:

$$\tau_{\rm Y}=\frac{a}{\dot{a}_{\rm Y}}=\frac{an}{2f_{\rm Y}\mathcal{F}}\simeq 160{\rm kyr}\left(\frac{r_{\rm p}}{1\ {\rm km}}\right)^2\left(\frac{r_{\rm s}}{0.2\ {\rm km}}\right)\left(\frac{a/r_{\rm p}}{2.5}\right)^{1/2}\left(\frac{0.005}{f_{\rm Y,0}}\right)\left(\frac{a_{\rm h}}{1\ {\rm au}}\right)^2, \quad (26)$$

where $f_{\rm Y,0}$ is the Yarkovsky coefficient at $a=2.5r_{\rm p}$. The Yarkovsky effect synchronizes the secondary by principally modifying its orbit, while the tidal and the YORP effects change its spin rate. Compared to the YORP timescale (Equation (25)), Equation (26) suggests that the Yarkovsky effect could operate more efficiently than the stochastic YORP for relatively large objects. The Yarkovsky could also dominate over the tidal effect unless the satellite is close in or large or the value μQ is smaller than assumed. Therefore, we propose that the Yarkovsky effect could be—at least in some small binaries—the major mechanism to synchronize the secondary. Let us give two examples of interest, namely, the Didymos–Dimorphos and Dinkinesh–Selam systems.

By abruptly reducing the binary orbit period, the NASA DART impact may have broken Dimorphos from synchronous rotation. Due to the oblate shape of Dimorphos (Daly et al. 2023), the spin–orbit coupling could be very weak, and instead of Dimorphos's long axis librating about the postimpact synchronous state, it could be circulating (Richardson et al. 2023). If this is the case, we can estimate the present Yarkovsky drift rate. By setting the orbital period to be 11.37 hr and the spin period to 12 hr, we obtained an estimate of $\dot{a}\sim 7.6\ {\rm cm\ yr^{-1}}$, which could be examined by the subsequent space mission ESA Hera that will launch in 2024 October to visit Didymos in fall 2026 (Michel et al. 2022). However, we note that this possibility is only one of many possible Dimorphos postimpact spin states, including tumbling (Agrusa et al. 2021; Richardson et al. 2023). The Yarkovsky effect does not vanish for tumbling objects (not even in the strong tumbling regime such as the long-axis mode). For a weak tumbling regime (short-axis mode), the Yarkovsky effect could be acceptably well represented using a traditional formulation (with rotation about the principal axis of the inertia tensor) and assuming (i) a spin axis oriented along the rotational angular momentum, (ii) a rotation period close to the precession period, and (iii) the shape given by the convex hull swept during the tumbling cycle (Vokrouhlický et al. 2015). There are many examples of tumbling NEAs, such as 99942 Apophis (Pravec et al. 2005, 2014; Vokrouhlický et al. 2015; Del Vigna et al. 2018; Pérez-Hernández & Benet 2022) and 4179 Toutatis (Vokrouhlický et al. 2005b; Chesley et al. 2015; Del Vigna et al. 2018), for which the Yarkovsky signal was firmly detected, pretty much as expected and within the expected range of the nontumbling state. Thus, we suspect that the rule of the Yarkovsky effect would still be valid for tumbling components in a binary system, while a more thorough investigation is required for confirmation in the future. There is some observational evidence indicating that Dimorphos may be in some excited tumbling state (Pravec et al. 2024), where the satellite's longest axis is approximately tidally locked to the direction toward the primary. Given its on average synchronous rotation, the Yarkovsky effect could be weak or even shut off in this case, but a more detailed analysis of this interesting system is needed.

In the latter case, the Dinkinesh–Selam binary recently discovered by the Lucy mission (Levison et al. 2024), the secondary asteroid Selam appears to be synchronous with a wide orbit at $a/r_{\rm p}\simeq 9$. Selam is likely a contact binary, possibly formed by the merger of two satellites. If this is the case, Selam was unlikely to be in synchronous rotation following a merger, requiring some synchronization mechanism to explain its present spin state. The timescale for the tidal despinning could be as long as $\sim$3 Gyr according to Equation (24), due to the wide orbit. However, the typical collisional lifetime of asteroids the size of Dinkinesh (0.8 km in diameter; Levison et al. 2024) is about 0.3 Gyr (Bottke et al. 2005). Since this lifetime is much smaller than the tidal despinning timescale, it is therefore unlikely that Selam was synchronized by the tidal effect, while the Yarkovsky effect can synchronize the orbit quickly. We found that the Yarkovsky timescale could be $\sim$1 Myr by setting $r_{\rm p}=720$ m, $r_{\rm s}=277$ m, $a=3.1$ km, $\rho_{\rm p}=\rho_{\rm s}=2.4\ {\rm g\ cm^{-3}}$, $a_{\rm h}=2.19$ au, and $e_{\rm h}=0.11$. Therefore, we propose that the Yarkovsky effect could be the main reason for its current synchronous state.

3.2. Long-term Evolution of Binary Asteroids

Let us now consider the possible evolutionary pathways of small binary systems in general terms, extending the canonical view (with tides and BYORP operating) by the Yarkovsky effect. Assume the parent body of the binary is disrupted either by

rotational fission or a catastrophic collision. The resulting fragments that are bound to the parent body accumulate to form a satellite, which can be either in synchronous or asynchronous rotation (Agrusa et al. 2024). The synchronous secondary evolves under the tidal and BYORP effects, resulting in a final state at the tide–BYORP equilibrium location (given that the BYORP torque is negative) or in a migration outward until it leaves the system or becomes chaotic (if the BYORP torque is positive) (Ćuk 2007; Ćuk & Nesvorný 2010; Jacobson & Scheeres 2011; Jacobson et al. 2014). Assuming a_{B-t} is the location of the BYORP–tide equilibrium, where $\dot{a}_B = -\dot{a}_t$, secondaries with a large BYORP coefficient f_B such that $a_{B-t} < a_{Roche}$ will cross the Roche limit and get tidally disrupted (Ćuk & Nesvorný 2010).

If the secondary is born asynchronous or perturbed into such a rotation state, it will evolve under the joint effect of tides and the Yarkovsky effect. If it happens to be in a spin–orbit resonance, BYORP is also active (Jacobson et al. 2014). For retrograde rotators, both tides and the Yarkovsky effect expand the secondary's semimajor axis until it is lost, forming an asteroid pair. The timescale for this process is $\min(\tau_t, \tau_Y) \lesssim \tau_Y$, considering that the strength of tides declines rapidly with the semimajor axis. In this case, the two components of the asteroid pair have opposite spin poles, different from asteroid pairs produced by rotational fission (Pravec & Scheirich 2010; Pravec et al. 2019) or BYORP (Ćuk 2007). For prograde rotators, the Yarkovsky effect will shrink the orbit if the secondary spins faster than the mean motion. If the secondary has a spin period P shorter than the orbital period at the Roche limit P_{Roche}, which is given by

$$P_{Roche} = 2\pi\sqrt{\frac{3}{4\pi G\rho_p}}\left(\frac{a_{Roche}}{r_p}\right)^{3/2} \simeq 4.3\ \mathrm{hr}\left(\frac{a_{Roche}}{1.5r_p}\right)^{3/2}, \quad (27)$$

then the secondary will migrate to this point and undergo significant reshaping or even tidal disruption. The typical Roche radius is given as $\sim 1.5\ r_p$ (Holsapple & Michel 2006), assuming the binary components have equal density. The traditional hydrostatic Roche radius is roughly $2.46\ r_p$, corresponding to an orbital period of ∼9 hr. The distribution of orbital periods of known binary systems shows a cutoff at 11 hr (Pravec et al. 2006). More recently confirmed binaries have confined the cutoff orbital period to 10.5 hr, suggesting that the Roche radius could be $2.7\ r_p$ for rubble piles with a weak structure or low density if the cutoff in the orbital period distribution is caused by tidal disruption. If the secondary has sufficient material strength (e.g., small monoliths), it is also possible that it would continue migrating inward and form a contact binary. Note that this process requires the Yarkovsky effect to overcome the outward torque due to tides. The semimajor axis a_{Y-t}, where tides balance the Yarkovsky effect, can be obtained by equating Equations (1)–(18):

$$a_{Y-t} = 0.84\ r_p\left(\frac{r_s}{0.2\ \mathrm{km}}\right)^{4/7}\left(\frac{0.005}{f_Y}\right)^{1/7}\left(\frac{10^{11}\mathrm{Pa}}{\mu Q}\right)^{1/7}. \quad (28)$$

This implies that the Yarkovsky effect easily overcomes tides for small binaries unless the tidal effect is much stronger than assumed. Changing f_Y to f_B makes the above equation for a_{B-t}. Considering the uncertainty of the tidal effect, we assume that a_{B-t} and a_{Y-t} could be located either inside or outside the a_{Roche}. If $a_{Y-t} > a_{Roche}$, the secondary will be stopped outside the Roche limit and be in a Yarkovsky–tide equilibrium state. However, this state can only last for a YORP timescale or a tidal despinning timescale, as the YORP torque or tides change the spin to shut off the Yarkovsky effect. For rotators with $P > P_{Roche}$, the Yarkovsky effect will move the secondary toward the synchronous orbit a_{syn}, except in the special case where the Yarkovsky effect is negative and balanced by tides, leading to a temporary Yarkovsky–tide equilibrium state at a_{Y-t}.

To summarize, we provide some predictions on the secondary dynamical state based on the Yarkovsky effect: (1) retrograde secondaries should be relatively far from the primaries; (2) some asteroid pairs could have opposite spin directions if they are formed by the Yarkovsky effect; (3) secondaries with a period shorter than the orbital period at the Roche radius, ranging from ∼4 to ∼10 hr, should be destroyed in a Yarkovsky timescale (∼0.1 Myr), otherwise they should be in a Yarkovsky–tide equilibrium (asynchronous) that lasts for a YORP timescale; and (4) secondaries with a period longer than the Roche orbital period should become synchronous after a Yarkovsky timescale.

3.3. Predicted Orbital Drift Rates of Real Binary Asteroids

As of now, there are 66 binary asteroid systems with documented secondary spin periods (Pravec & Harris 2007; Warner et al. 2009; Pravec et al. 2012, 2016; Monteiro et al. 2023). Among these, five are known to exhibit spin periods that are different from their orbital periods to date. While there are other potentially asynchronous binary systems, their information is either undetermined or incomplete (Pravec et al. 2016). Consequently, we computed the theoretical Yarkovsky drift rates for these five asynchronous binary asteroids for future tests.

It is important to note that the Yarkovsky effect remains applicable to those binary systems with $n = \omega$, provided their obliquity is nonzero. However, due to insufficient data on the spin vectors, the information regarding the axial tilt of real asteroids remains ambiguous. Here our focus is limited to asteroids with $n \neq \omega$, for which BYORP does not work. We estimated the Yarkovsky effect for these bodies in the limiting cases $\varepsilon = 0°$ and 180°. The result is shown in Table 1. We notice that there are a few asteroid binaries (e.g., Esclangona, Arlon) with a large separation, although their spin periods are much smaller than the orbital periods ($m \ll 1$). This large separation was explained as a result of the BYORP-induced expansion and subsequent desynchronization (Jacobson et al. 2014). We found that the Yarkovsky effect could also expand the mutual orbit, if the secondaries have obliquities around or larger than 90°, which is left for future observational tests. The Yarkovsky effect decreases with increasing separation, not only because of the decreasing time fraction in the shadow over a mutual orbit (i.e., c_1 in Equations (6) and (7)) but also due to the challenges in maintaining the shadow condition over the heliocentric orbit. For a distant satellite, the inclination of its orbit about the primary should be confined in a narrower interval of values than for close satellites. Accounting for the potential nonexistence of the shadow in a relatively high-inclination heliocentric orbit, the c_1 should be revised as the time fraction that the secondary spends in the shadow over a heliocentric orbit.[7] Therefore, thorough orbital modeling is crucial for assessing the Yarkovsky drift rates for distant satellites. The predictions provided by Table 1 are based on the

[7] This reduces to $c_1 \simeq r_p/\pi a$ when $i = 0$.

Table 1
The Yarkovsky Effect Predicted for Known Asynchronous Binaries

Name	a_h (au)	e_h	r_p (km)	r_s/r_p	a/r_p	P_{orb} (hr)	P_s (hr)	f_Y ($\times 10^{-3}$)	$\dot{a}_Y$ (cm yr^{-1})
(1509) Esclangona	1.866	0.032	4.25	0.33	49.2	768	6.6422	−0.54/+0.41	−0.52/+0.39
(2486) Metsahovi	2.269	0.08	4	0.30	18.3	172.6	2.64	−0.97/+1.0	−0.17/+0.17
(2623) Zech	2.255	0.234	3.4	0.29	14.1	117.2	18.718	−2.0/+1.7	−0.29/+0.25
(32039) 2000 JO23	2.223	0.283	1.3	0.65	33.1	360	11.09	−0.81/+0.67	−0.45/+0.37
(311066) 2004 DC	1.634	0.400	0.15	0.20	4.6	23	7	−5.3/+4.6	−10.2/+9.0

Note. The orbital period of the binary components relative to each other is $P_{orb} = 2\pi/n$, while the rotation period of the secondary is $P_s = 2\pi/\omega$. The Yarkovsky coefficient f_Y and the drift rate a_Y are calculated for an obliquity equal to 0°/180°. The thermal parameters are assumed to be the same as those used in Section 2.2. It is important to note that for the distant satellites, the Yarkovsky effect could be diminished (see Section 3.3).

simplest situations and therefore only give the upper limits of Yarkovsky drift rates.

There are also some binaries (e.g., 1994 CC, 2001 SN263, 2004 DC, etc.) with large heliocentric eccentricities; therefore, they may also suffer from strong planetary perturbations that modify the mutual orbit and the spin state. Since the Yarkovsky effect is much more deterministic than the BYORP effect once the rotational state is known, our hypotheses can be easily examined by future observations.

4. Conclusions

The Yarkovsky effect is the radiative force acting on a rotating object with nonzero thermal inertia, gradually altering its orbit over the long term. In this work, we investigate the Yarkovsky effect on a binary asteroid system. The binary Yarkovsky effect, manifesting primarily on the secondary asteroid, comprises two main components: the YS effect and the planetary Yarkovsky effect. The former is the net Yarkovsky force averaged over the mutual orbital period due to the eclipse caused by the primary on the secondary. As a result of the eclipse condition, the YS effect is only significant for low-inclination binary asteroids (e.g., $i < r_p/a$), which are common in both the NEA and MBA populations. The planetary Yarkovsky effect is simply produced by the radiation from the primary asteroid instead of the Sun. For low-inclination asteroids, the YS effect dominates over the planetary Yarkovsky effect. The direction of the binary Yarkovsky effect depends on the obliquity and the difference between the spin rate and the mean motion of the secondary, while the magnitude depends on the thermal and orbital properties of the binary system. In general, the binary Yarkovsky effect moves the secondary to make the mean motion match the spin rate on a timescale of ∼0.1 Myr.

We found that for prograde-rotating secondaries, the Yarkovsky effect can synchronize the secondary (i.e., $\omega = n$) by orbit modification on a timescale much shorter than tidal despinning, except for large or close-in secondaries. On the other hand, the YORP effect could be more efficient for synchronization of small secondaries. This is because of its timescale depending on $\sim r_s^2$ rather than $\sim r_s$ for the Yarkovsky effect. This brings us new insights about the mechanism of the synchronization of binary asteroids and the underlying reason why the majority of binary asteroids are found to be in synchronous states. Our calculations also predict that the secondary asteroids with spin periods shorter than the orbital period around the Roche limit (e.g., from ∼4 to ∼10 hr) will fall into the Roche limit quickly driven by the Yarkovsky effect and then get tidally disrupted, reshaped, or accreted on the primary. In addition, some asynchronous binaries might be in the Yarkovsky–tide equilibrium state where the orbit does not drift, but such a state may be quickly broken by the YORP effect or tides. For retrograde secondaries, the Yarkovsky effect would drive them outward until they leave the binary system due to planetary perturbations or collisions, producing asteroid pairs. In this scenario, the two components of the asteroid pair would exhibit opposite spin directions.

We also calculated the Yarkovsky-caused drift rate for known asynchronous binaries, listed in Table 1 for future observational tests. Some of the asynchronous binary asteroids have wide mutual orbits, which could be the result of the Yarkovsky effect on retrograde secondaries. We found that the synchronization of the Dinkinesh–Selam system discovered by the Lucy spacecraft could be due to the Yarkovsky effect, considering that tides are weak for such a distant secondary. In addition, we calculated the possible Yarkovsky effect on the Didymos–Dimorphos system in its state following the impact of the NASA DART mission, which might have perturbed it into an asynchronous state. The Yarkovsky coefficient f_Y is around 0.0067, and the resulting semimajor axis drift rate is $\dot{a} \simeq 7.6$ cm yr^{-1}. This could be examined by in situ observation conducted by the space mission ESA Hera during its rendezvous with Didymos in late 2026.

Acknowledgments

We thank Miroslav Brož and Jay McMahon for useful discussions and the referee whose comments helped to improve the submitted manuscript. We acknowledge support from the Université Côte d'Azur. W.-H.Z. would like to acknowledge the funding support from the Chinese Scholarship Council (No. 202110320014). The work of D.V. and P.P. was partially supported by the Czech Science Foundation (grant 23-04946S). M.K. acknowledges the funding support by the JSPS KAKENHI No. JP22J00435/JP22KJ0728 and MEXT Promotion of Distinctive Joint Research Center Program grant No. JPMXP0622717003/JPMXP0723830458. H.A. was supported by the French government through the UCA J.E.D.I. Investments in the Future project managed by the National Research Agency (ANR) with the reference number ANR-15-IDEX-01. P.M. acknowledges funding support from the French space agency (CNES) and the European Space Agency (ESA).

Appendix A
Nomenclature

The symbols used in this Letter are listed in Table 2.

Table 2
Notation Used throughout This Letter

Symbols		Subscripts	
a	Semimajor axis of a mutual orbit	p	Primary component of a binary asteroid
k	Love number	s	Secondary component of a binary asteroid
n	Mean motion	h	Heliocentric parameter
Q	Quality factor	B	BYORP
r	Radius	Y	Yarkovsky
f	Dimensionless coefficient	YS	Yarkovsky–Schach
A	Bond albedo	pY	Planetary Yarkovsky
ρ	Density	Y-t	Yarkovsky–tide equilibrium
μ	Rigidity	B-t	BYORP–tide equilibrium
i	Inclination	Roche	Roche limit
ε	Obliquity		
ω	Spin rate of the secondary		
τ	Timescale		
Θ	Thermal parameter		
Γ	Thermal inertia		
$\mathcal{F}$	Nominal radiative force per unit mass		

Appendix B
Functions $A(x)$, $B(x)$, $C(x)$, and $D(x)$

The functions $A(x)$, $B(x)$, $C(x)$, and $D(x)$, useful to express the $V(z)$ in real notation (Equation (11)), are given by (e.g., Vokrouhlický 1998, 1999)

$$A(x) = -(x+2) - e^x[(x-2)\cos x - x\sin x], \tag{B1}$$

$$B(x) = -x - e^x[x\cos x + (x-2)\sin x], \tag{B2}$$

$$a(x) = 3(x+2) + e^x[3(x-2)\cos x + x(x-3)\sin x], \tag{B3}$$

$$b(x) = x(x+3) - e^x[x(x-3)\cos x - 3(x-2)\sin x], \tag{B4}$$

with $C(x) = A(x) + \chi\, a(x)/(1+\chi)$ and $D(x) = B(x) + \chi\, b(x)/(1+\chi)$.

Appendix C
Special Cases for $f_{\rm Y}$

The formula of the Yarkovsky coefficient $f_{\rm Y}$ can be simplified in some special cases. In the fast spin regime, where $\omega \gg n$ such that $m \gg 1$, $V(z_{m+1}) \simeq V(z_{m-1}) \simeq V(z_m)$ and $z_m = \sqrt{-\imath m}\ r_{\rm s}/l_n$. In this case, one could replace the penetration depth l_n of the thermal wave at mean-motion frequency n with a penetration depth $l_d = l_n/\sqrt{m}$ of the thermal wave at rotation frequency, thence $z_m = \sqrt{-\imath}\ r_{\rm s}/l_d$. Since $\cos^4(\varepsilon/2) - \sin^4(\varepsilon/2) = \cos\varepsilon$, we obtain a simpler form of Equation (6) reading

$$f_{\rm YS,d} = \frac{4c_1}{9} V(z_m)\cos\varepsilon. \tag{C1}$$

This equation resembles the classic Yarkovsky effect for a single asteroid orbiting around the Sun but is multiplied by $-c_1$. Therefore, the Yarkovsky is maximized when the spin thermal parameter $\Theta_\omega \sim \sqrt{2}$, which is defined as

$$\Theta_\omega = \frac{\Gamma\sqrt{\omega}}{\varepsilon\sigma T_{\rm sub}^3} \sim \sqrt{2}\left(\frac{\Gamma}{200\ \mathrm{J\ m^{-2}\ K^{-1}\ s^{-1/2}}}\right) \times \left(\frac{P_{\rm s}}{3\ \mathrm{hr}}\right)^{-1/2}\left(\frac{a_{\rm h}}{1\ \mathrm{au}}\right)^{3/2}. \tag{C2}$$

It is obvious that when $\varepsilon = 0°$, there is only the diurnal component left, leading to the inward migration of the secondary asteroid and the decrease of m (since n becomes larger).

In the slow spin regime, where $\omega \ll n$ such that $m \sim 0$, we have $V(z_{m+1}) \simeq -V(z_{m-1}) \simeq V(z_1)$ and $z_1 = \sqrt{-\imath}\ r_{\rm s}/l_n$. Therefore,

$$f_{\rm YS,d} = -\frac{4c_1}{9} V(z)\left(1 - \frac{1}{2}\sin^2\varepsilon\right). \tag{C3}$$

Interestingly, when combined with the seasonal component, we get the total YS coefficient $f_{\rm YS}$,

$$f_{\rm YS} = -\frac{4c_1}{9} V(z_1), \tag{C4}$$

that is independent of the obliquity ε. Here, $f_{\rm YS} > 0$, which leads to an outward migration and increasing m (since n becomes smaller).

In the synchronous regime where $m = 1$, considering $V(z_0) \to 0$, we obtain

$$f_{\rm YS,d} = \frac{4c_1}{9} V(z_{-2})\sin^4\frac{\varepsilon}{2}, \tag{C5}$$

and $f_{\rm YS,s}$ remains the same. This will result in a zero Yarkovsky effect given that $\varepsilon = 0°$. For the case of $\varepsilon \neq 0°$, the Yarkovsky effect always transfers a positive angular momentum, driving the secondary outward.

ORCID iDs

Wen-Han Zhou (周文翰) https://orcid.org/0000-0003-4229-8936
David Vokrouhlický https://orcid.org/0000-0002-6034-5452
Masanori Kanamaru https://orcid.org/0000-0002-2533-3077
Harrison Agrusa https://orcid.org/0000-0002-3544-298X
Petr Pravec https://orcid.org/0000-0001-8434-9776
Marco Delbo https://orcid.org/0000-0002-8963-2404
Patrick Michel https://orcid.org/0000-0002-0884-1993

References

Agrusa, H. F., Gkolias, I., Tsiganis, K., et al. 2021, Icar, 370, 114624
Agrusa, H. F., Zhang, Y., Richardson, D. C., et al. 2024, PSJ, 5, 54
Bottke, W. F., Durda, D. D., Nesvorný, D., et al. 2005, Icar, 175, 111
Bottke, W. F., Vokrouhlický, D., Rubincam, D. P., & Nesvorný, D. 2006, AREPS, 34, 157
Bottke, W. F., Vokrouhlický, D., Walsh, K. J., et al. 2015, Icar, 247, 191
Breiter, S., Bartczak, P., Czekaj, M., Oczujda, B., & Vokrouhlický, D. 2009, A&A, 507, 1073
Burns, J. A., & Safronov, V. S. 1973, MNRAS, 165, 403
Caudal, G. 2023, Icar, 402, 115606
Chesley, S., Farnocchia, D., Pravec, P., & Vokrouhlický, D. 2015, IAUGA, 29, 2248872
Cotto-Figueroa, D., Statler, T. S., Richardson, D. C., & Tanga, P. 2015, ApJ, 803, 25
Ćuk, M. 2007, ApJL, 659, L57

Ćuk, M. 2023, AAS/Division of Dynamical Astronomy Meeting, 55, 501.01
Ćuk, M., & Burns, J. A. 2005, Icar, 176, 418
Ćuk, M., Jacobson, S. A., & Walsh, K. J. 2021, PSJ, 2, 231
Ćuk, M., & Nesvorný, D. 2010, Icar, 207, 732
Daly, R. T., Ernst, C. M., Barnouin, O. S., et al. 2023, Natur, 616, 443
Del Vigna, A., Faggioli, L., Milani, A., et al. 2018, A&A, 617, A61
DellaGiustina, D. N., Ballouz, R. L., Walsh, K. J., et al. 2024, MNRAS, 528, 6568
Durda, D. D., Bottke, W. F., Enke, B. L., et al. 2004, Icar, 170, 243
Ďurech, J., Vokrouhlický, D., Pravec, P., et al. 2024, A&A, 682, A93
Efroimsky, M. 2015, AJ, 150, 98
Farinella, P., & Vokrouhlický, D. 1996, P&SS, 44, 1551
Gladman, B., Michel, P., & Froeschlé, C. 2000, Icar, 146, 176
Goldreich, P., & Sari, R. 2009, ApJ, 691, 54
Golubov, O., & Krugly, Y. N. 2012, ApJL, 752, L11
Holsapple, K. A., & Michel, P. 2006, Icar, 183, 331
Jacobson, S. A., & Scheeres, D. J. 2011, ApJL, 736, L19
Jacobson, S. A., Scheeres, D. J., & McMahon, J. 2014, ApJ, 780, 60
Kanamaru, M., Sasaki, S., Morota, T., et al. 2021, JGRE, 126, e06863
Levison, H., et al. 2024, Natur, 629, 1015
Marzari, F., Rossi, A., Golubov, O., & Scheeres, D. J. 2020, AJ, 160, 128
McMahon, J., & Scheeres, D. 2010, Icar, 209, 494
Michel, P., Benz, W., Tanga, P., & Richardson, D. C. 2001, Sci, 294, 1696
Michel, P., Küppers, M., Bagatin, A. C., et al. 2022, PSJ, 3, 160
Milani, A., Nobili, A. M., & Farinella, P. 1988, AN, 309, 38
Monteiro, F., Lazzaro, D., Rondón, E., et al. 2023, Icar, 390, 115297
Murawiecka, M., & Lemaitre, A. 2018, AdSpR, 61, 935
Murray, C. D., & Dermott, S. F. 1999, Solar System Dynamics (Cambridge: Cambridge Univ. Press)
Naidu, S. P., Chesley, S. R., Moskovitz, N., et al. 2024, PSJ, 5, 74
Nesvorný, D., Youdin, A. N., & Richardson, D. C. 2010, AJ, 140, 785
Pérez-Hernández, J. A., & Benet, L. 2022, ComEE, 3, 10
Pou, L., & Nimmo, F. 2024, Icar, 411, 115919
Pravec, P., Fatka, P., Vokrouhlický, D., et al. 2019, Icar, 333, 429
Pravec, P., & Harris, A. W. 2007, Icar, 190, 250
Pravec, P., Harris, A. W., Scheirich, P., et al. 2005, Icar, 173, 108
Pravec, P., & Scheirich, P. 2010, AAS/Division for Planetary Sciences Meeting Abstracts, 42, 13.13
Pravec, P., Scheirich, P., Ďurech, J., et al. 2014, Icar, 233, 48
Pravec, P., Scheirich, P., Kušnirák, P., et al. 2006, Icar, 181, 63
Pravec, P., Scheirich, P., Kušnirák, P., et al. 2016, Icar, 267, 267
Pravec, P., Scheirich, P., Meyer, A., et al. 2024, Icar, 418, 116138
Pravec, P., Scheirich, P., Vokrouhlický, D., et al. 2012, Icar, 218, 125
Quillen, A. C., LaBarca, A., & Chen, Y. 2022, Icar, 374, 114826
Richardson, D., Agrusa, H., Barbee, B., et al. 2023, LPI Contribution, 2851, 2040
Rozitis, B., & Green, S. F. 2012, MNRAS, 423, 367
Rubincam, D. P. 1982, CeMec, 26, 361
Rubincam, D. P. 1987, JGR, 92, 1287
Rubincam, D. P. 2000, Icar, 148, 2
Rubincam, D. P. 2006, Icar, 184, 532
Scheirich, P., & Pravec, P. 2022, PSJ, 3, 163
Scheirich, P., Pravec, P., Jacobson, S. A., et al. 2015, Icar, 245, 56
Scheirich, P., Pravec, P., Kušnirák, P., et al. 2021, Icar, 360, 114321
Scheirich, P., Pravec, P., Meyer, A. J., et al. 2024, PSJ, 5, 17
Statler, T. S. 2009, Icar, 202, 502
Steinberg, E., & Sari, R. 2011, AJ, 141, 55
Taylor, P. A., & Margot, J.-L. 2011, Icar, 212, 661
Vokrouhlický, D. 1998, A&A, 335, 1093
Vokrouhlický, D. 1999, A&A, 344, 362
Vokrouhlický, D., Bottke, W. F., Chesley, S. R., Scheeres, D. J., & Statler, T. S. 2015, in Asteroids IV, ed. P. Michel, F. E. DeMeo, & W. F. Bottke (Tucson, AZ: Univ. of Arizona Press), 509
Vokrouhlický, D., Čapek, D., Chesley, S. R., & Ostro, S. J. 2005a, Icar, 179, 128
Vokrouhlický, D., Čapek, D., Chesley, S. R., & Ostro, S. J. 2005b, Icar, 173, 166
Vokrouhlický, D., Farnocchia, D., Čapek, D., et al. 2015, Icar, 252, 277
Vokrouhlický, D., Nesvorný, D., Dones, L., & Bottke, W. F. 2007, A&A, 471, 717
Walsh, K. J., & Jacobson, S. A. 2015, in Asteroids IV, ed. P. Michel, F. E. DeMeo, & W. F. Bottke (Tucson, AZ: Univ. of Arizona Press), 375
Walsh, K. J., Richardson, D. C., & Michel, P. 2008, Natur, 454, 188
Warner, B. D., Harris, A. W., & Pravec, P. 2009, Icar, 202, 134
Yoder, C. F. 1982, Icar, 49, 327
Zhou, W.-H., & Michel, P. 2024, A&A, 682, A130
Zhou, W.-H., Zhang, Y., Yan, X., & Michel, P. 2022, A&A, 668, A70